Diversity of Omega Glutathione Transferases in mushroom-forming fungi revealed by phylogenetic, transcriptomic, biochemical and structural approaches

Thomas Perrot, Mathieu Schwartz, Aurélie Deroy, Jean-Michel Girardet, Annegret Kohler, Melanie Morel-Rouhier, Frédérique Favier, Éric Gelhaye, Claude Didierjean

Title

Diversity of Omega Glutathione Transferases in mushroom-forming fungi revealed by phylogenetic, transcriptomic, biochemical and structural approaches

Authors' names

Thomas Perrot[a,c,1], Mathieu Schwartz[b,d,1], Aurélie Deroy[a], Jean-Michel Girardet[a], Annegret Kohler[a], Mélanie Morel-Rouhier[a], Frédérique Fa vier[b], Eric Gelhaye[a*], Claude Didierjean[b*]

1 Thomas Perrot and Mathieu Schwartz contributed equally to this work.

Addresses.

a Université de Lorraine, INRAE, IAM, Nancy, France.

b Université de Lorraine, CNRS, CRM2, Nancy, France.

c Institute for Plant Cell Biology and Biotechnology, Heinrich Heine University, 40225 Düsseldorf, Germany

d CSGA, UMR1324 INRAE, UMR6265 CNRS, Université de Bourgogne, Agrosup Dijon, Dijon, France

***Corresponding authors :**

Eric Gelhaye, Université de Lorraine, INRAE, IAM, Nancy, France, eric.gelhaye@univ-lorraine.fr, Tel. +336 04 52 03 80, https://mycor.nancy.inra.fr/IAM/

Claude Didierjean, Université de Lorraine, CNRS, CRM2, Nancy, France, claude.didierjean@univ-lorraine.fr, Tel. +333 72 74 56 42, http://crm2.univ-lorraine.fr/lab/fr/

Abstract

The Omega class of glutathione transferases (GSTs) forms a distinct class within the cytosolic GST superfamily because most of them possess a catalytic cysteine residue. The human GST Omega 1 isoform was first characterized twenty years ago, but it took years of work to clarify the roles of the human isoforms. Concerning the kingdom of fungi, little is known about the cellular functions of Omega glutathione transferases (GSTOs), although they are widely represented in some of these organisms. In this study, we re-assess the phylogeny and the classification of GSTOs based on 240 genomes of mushroom-forming fungi (Agaricomycetes). We observe that the number of GSTOs is not only extended in the order of Polypores but also in other orders such as Boletales. Our analysis leads to a new classification in which the fungal GSTOs are divided into two Types A and B. The catalytic residue of Type-A is either cysteine or serine, while that of Type-B is cysteine. The present study focuses on *Trametes versicolor* GSTO isoforms that possess a catalytic cysteine residue. Transcriptomic data show that Type-A GSTOs are constitutive enzymes while Type-B are inducible ones. The crystallographic analysis reveals substantial structural differences between the two types while they have similar biochemical profiles in the tested conditions. Additionally, these enzymes have the ability to bind antioxidant molecules such as wood polyphenols in two possible binding sites as observed from X-ray structures. The multiplication of GSTOs could allow fungal organisms to adapt more easily to new environments.

Keywords

Glutathione transferase, glutathione, flavonoid, enzyme, structure-function, fungi

1 Introduction

Wood-decay fungi have the ability to degrade and mineralize all the wood components, and therefore are of great importance in organic matter recycling and potential valorization in many industrial domains. Recently, genomic comparative analysis has highlighted the co-evolution of genes involved in the extracellular oxidation and in the intracellular detoxification systems in the fungal wood degradation process (Nagy et al., 2016). These organisms show expansion of multigenic families involved in oxidation such as cytochrome P450 mono-oxygenases and in conjugation such as cytosolic glutathione transferases (GSTs) (Morel et al., 2013; Syed et al., 2014), which are part of conjugation and sequestration/secretion that achieves intracellular detoxification.

GSTs are widespread enzymes, which use glutathione (GSH) through different reactions (Deponte, 2013; Hayes et al., 2005). GSTs that harbor a serine residue or a tyrosine residue exhibit generally glutathione-transferase activity, while GSTs with a cysteine residue mainly possess deglutathionylating activity (Lallement et al., 2014a). Some GSTs also have storage or transport roles through their ability to bind non-catalytically metabolites or xenobiotics at their ligandin binding site (Ahmad et al., 2017; McTigue et al., 1995). The fungal GST family is subdivided into seven classes and three of them are expanded in wood-decay fungi: the GSTFuA class (Mathieu et al., 2012; Mathieu et al., 2013; Osman et al., 2018), the GST Ure2p (Roret et al., 2015; Thuillier et al., 2013) and the GST Omega (GSTO) (Meux et al., 2013). Exploration of the genome of the white-rot *Trametes versicolor* suggests expansion of the classes GSTO (coded by 16 genes among the 45 genes coding for GSTs) (Deroy et al., 2015) and Ure2p (coded by 11 genes). Based on 22 fungal genomes, Omega-related sequences were previously clustered into three distinct subclasses I, II and III (Morel et al., 2009). The characterization of bacterial and fungal isoforms of the Omega-subclass I revealed unambiguously that it constitutes a new class of GSTs named Xi class (GSTX) (Meux et al., 2011). Cysteine GSTOs from *Phanerochaete chrysosporium* (PcGSTO3C and PcGSTO4C) reduce disulfide substrates and glutathione derivatives (Meux et al., 2013; Meux et al., 2011). Serine GSTOs from *T. versicolor* and *P. chrysosporium* catalyze the glutathione conjugation of usual GST substrates (Deroy et al., 2015). Using ligand-fishing strategies, we demonstrated at the biochemical and structural levels that these serine GSTOSs interact with polyphenolic compounds from wood species, such as oxyresveratrol, a well-known potent antioxidant (Perrot et al., 2018; Schwartz et al., 2018). Our data suggest a role for GSTOs in the transport and sequestration of flavonoids and indicate that they could be used to detect wood-molecules of potential interest.

Fungal GSTOs have animal homologs that have been extensively studied (Board, 2011; Board and Menon, 2016; Whitbread et al., 2005). In short, animals GSTOs have a catalytic cysteine residue in their active site and exhibit lyase activity (i.e. deglutathionylation) with glutathione derivatives and even glutathionylated proteins. Human GSTO1 (HsGSTO1) was found to be involved in the glutathionylation cycle, pro-inflammatory signaling and cancer drug resistance. Recently, **Hughes** et al. provide evidence for HsGSTO1 as a regulator of the inflammasome NLRP3 through deglutathionylation of a protein (Hughes et al., 2019). HsGSTO1 is today a potential therapeutic target for wide-range inflammation-related diseases (Xie et al., 2020).

In the present study, the classification of the Omega GSTs in mushroom-forming fungi (Agaricomycetes) was upgraded from 240 genomes. We show that fungal GSTOs can be divided phylogenetically in two clades, named Type-A and Type-B GSTOs. Type-A GSTOs have either serine or

cysteine residue in their active site while Type-B GSTOs contains only cysteine residue. We report for the first time an in-depth structure function analysis of *T. versicolor* Type-A and B GSTOs that contain a catalytic cysteine residue. Both types show significant differences in their expression levels and in their three-dimensional structures, but they retain similar catalytic profiles and the ability to bind wood polyphenols like serine TvGSTOs.

2 Material and Methods

2.1 Materials

1,4-dithiothreitol (DTT) was bought from Euromedex (Souffelweyersheim, France). L-glutathione reduced (GSH), phenethyl isothiocyanate (PEITC), benzyl isothiocyanate (BEITC), cumene hydroperoxide (CuOOH), pinocembrin (PINO), scutellarein (SCUT), baicalein (BAIA), chrysin (CHRY), naringenin (NARE), catechin hydrate (CATE), quercetin (QUER), oxyresveratrol (OXYR) and naringin (NARI) were purchased from Sigma-Aldrich (Steinheim, Germany). 1-chloro-2,4-dinitrobenzene (CDNB), 2-hydroxyethyl disulfide (HED) and **5,5-dithio-bis-(2-nitrobenzoic acid)** (Ellman's reagent or DTNB) were purchased from Acros Organics (Geel, Belgium). Wogonin (WOGO) and wogonoside (WOSI) have been purchased from Extrasynthese (Genay, France) and Abcam (Cambridge, England, United Kingdom), respectively. The tested glutathionylated substrate, S-glutathionyl-phenylacetophenone (GS-PAP) has been in vitro synthesized as previously described (Vince et al., 1971).

2.2 Transcriptomic analysis

Mycelia of *Trametes versicolor* BRFM1218 and *Trametes versicolor* 1956-1252 (NIBIO collection) were harvested after 2 and 4 weeks of incubation on 4% malt agar medium. Total RNA was extracted and purified from triplicate cultures using the RNeasy plant miniKit as described previously (Thuillier et al., 2014). Preparation of libraries from total RNA and 2 x 100bp Illumina HiSeq sequencing (RNA-Seq) was performed at the Beckman Coulter Genomic facilities.

Raw reads were trimmed and aligned to the *Trametes versicolor* reference transcripts available at the JGI MycoCosm database (http://genome.jgi-psf.org/programs/fungi/index.jsf) using CLC Genomics Workbench v8. For mapping, the minimum length fraction was 0.9, the minimum similarity fraction 0.8 and the maximum number of hits for a read was set to 10. The unique and total mapped reads number for each transcript were determined, and then normalized to RPKM (Reads Per Kilobase of exon model per Million mapped reads). Intact pairs were counted as two, broken pairs as one. The complete data sets were submitted to GEO (GSE154077). **The Baggerly's test included in CLC Genomic workbench was applied to the data to identify differentially regulated transcripts.** In addition, Benjamini & Hochberg multiple-hypothesis testing corrections with False Discovery Rate (FDR) were used.

2.3 Comparative genomic and phylogenetic analysis

A comparative genomic analysis was performed on 240 sequenced fungal genomes that belong to the clade of Agaricomycotina. This analysis has been carried out by using the Mycocosm database from the Joint Genome Institute (at the date of 16/10/2017). Fungal omega GSTs sequences have been recovered by using the peptide sequence of TvGSTO3S (Prot ID "48691 ", Type-A) and TvGSTO3C (Prot ID "60698 ", Type-B) with the Basic Local Alignment Search Tool in the JGI website

(BLAST). To check the affiliation of sequences to the Omega class, the sequences were aligned with the MEGA software (version 6, CLUSTALW) (Tamura et al., 2013) and the sequence identity were determined by using MatGAT software (Campanella et al., 2003). In comparison with the Omega class, another genomic analysis of the Xi class has been carried out with the same methodology by using the peptide sequences of TvGSTX1 (Prot ID "66368"), TvGSTX2 (Prot ID "50990" and TvGSTX3 (Prot ID "73942") as templates with the BLAST. A phylogenetic analysis of Omega and Xi class has been performed on ten fungal genomes from various orders and that have a high number of genes coding for GSTOs. The selected sequences were aligned using the MAFFT program and a phylogenetic tree was constructed using the neighbor-joining method with the bootstrap resampling number set at 1000 (Rozewicki et al., 2019). The phylogenetic tree was visualized using iTOL (Letunic and Bork, 2019).

2.4 Production and purification

The production in *Escherichia coli* (Rosetta2 DE3 pLysS strain, Novagen) and purification of the nine selected TvGSTOs (accession number in the JGI database: TvGSTO1C: 157166; TvGSTO2C: 67635; TvGSTO3C: 60698; TvGSTO1S: Tv75639; TvGSTO2S: Tv56280; TvGSTO3S: Tv48691; TvGSTO4S: Tv65402; TvGSTO5S: Tv54358 and TvGSTO6S: Tv23671) were performed as explained previously (Deroy et al., 2015).

2.5 Crystallography

A first screening of 288 crystallization conditions was carried out at the CRM2 crystallogenesis platform (University of Lorraine) with Oryx 8 crystallogenesis robot (Douglas Instruments Ltd). Crystals were optimized manually at 4°C by the microbatch under oil method (TvGSTO2C and TvGSTO3C) or by the vapor diffusion hanging drop method (TvGSTO1C). TvGSTO1C was crystallized by mixing 1 µL of protein (11 mg/mL) with 1 µL of solution consisting in 10% (w/v) polyethylene glycol 8000 and 0.1 M pH 7.5 HEPES buffer, while the reservoir contained 1 mL of the same crystallization solution. TvGSTO2C was crystallized by mixing 1 µL of protein (19 mg/mL) with 1 µL of solution consisting in 20% (w/v) polyethylene glycol 4000, 10% (v/v) 2-Propanol and 0.1 M pH 7.5 HEPES buffer. TvGSTO3C was crystallized by mixing 1 µL of protein (13 mg/mL) with 1 µL of solution consisting in 15% (w/v) polyethylene glycol 8000 and 0.2 M ammonium sulfate. Crystals of TvGSTO2C-naringenin and TvGSTO2C-oxyresveratrol complexes were prepared by the 'dry soaking method' as explained previously (Perrot et al., 2018; Schwartz et al., 2018). Briefly, 0.1 µL of ligand (100 mM in DMSO) was used to coat each well of the plate and left to complete evaporation. Then, one TvGSTO2C crystal together with 1 µL of its mother liquor was dispensed on the dried ligand. After incubation (10 hours for oxyresveratrol; 2 months for naringenin), the crystals did not show severe damage and were flash frozen after a quick soaking in their mother liquor supplemented with 20% glycerol.

Preliminary X-ray diffraction experiments were carried out in-house on an Agilent SuperNova diffractometer (Oxford Diffraction) equipped with a CCD detector. Data collections were carried out at the ESRF, on beamline FIP BM30A and ID30B (Grenoble, France). Data sets were indexed and integrated with XDS (Kabsch, 2010), and scaled and merged with XSCALE or Aimless (Evans and Murshudov, 2013) from the CCP4 suite (Winn et al., 2011). The structure of TvGSTO1C was solved by molecular replacement using MOLREP (Vagin and Teplyakov, 2010) with the coordinates of TvGSTO3S from *Trametes versicolor* (PDB code 6F43) as the search model. The structures of

TvGSTO2C and TvGSTO3C were solved by molecular replacement using MOLREP with the coordinates of TvGSTO1C as the search model. In the structures of the complexes involving TvGSTO2C, electron density maps revealed unambiguously the presence of the ligands in binding pockets of the protein. Restraint files for naringenin and oxyresveratrol were generated with the GRADE server (URL http://grade.globalphasing.org/cgi-bin/grade/server.cgi). Structures were refined with PHENIX (Liebschner et al., 2019) and manually improved with COOT (Emsley and Cowtan, 2004). Validation of all structures was performed with MolProbity (Davis et al., 2004) and the PDB validation service (http://validate.wwpdb.org). Coordinates and structure factors have been deposited in the Protein Data Bank (PDB codes TvGSTO1C : 6HJS ; TvGSTO2C : 6SR8, TvGSTO2C/Naringenin : 6SRA ; TvGSTO2C/oxyresveratrol : 6SR9 and TvGSTO3C : 6SRB).

2.6 Reduction treatment on TvGSTO1C, TvGSTO2C and TvGSTO3C

The three native His6-tagged TvGSTOs were reduced by using 1,4-dithiothreitol (DTT). **An excess of DTT with a concentration ten times higher than that of the protein was added in a 30 mM Tris-HCl pH 8.0, 1 mM EDTA buffer.** After two hours of incubation at room temperature, the reduction reaction mixture was dialyzed at 4°C in a 30 mM Tris-HCl pH 8.0, 200 mM NaCl buffer in order to remove DTT.

2.7 Mass spectrometry analysis

Oxidized and reduced forms of His6-tagged TvGSTO1C, 2C and 3C were analyzed by direct introduction with electrospray ionization (ESI).

2.8 Determination of free thiol groups

To determine the number of free thiol groups in cysteine residues, we used a spectrophotometric method based on the cleavage of the Ellman's Reagent, 5,5-dithio-bis-(2-nitrobenzoic acid) (DTNB). Untreated and reduced forms of TvGSTO1, 2C and 3C (10 µM) were incubated with 200 µM of DTNB in 30 mM Tris-HCl pH 8.0, 1 mM EDTA, SDS 1% for a final volume of 500 µL. The reaction mixture was incubated at room temperature during thirty minutes in the dark. After that, the absorbance of each condition was measured at 412 nm. The concentration of TNB, corresponding to the cleavage product of DTNB, was calculated by dividing the absorbance measured with the molar absorption coefficient (εTNB = 13900 $M^{-1}.cm^{-1}$). Then, the ratio between the concentrations of TNB and protein gave the number of free thiol group. For each condition, two replicates have been made.

2.9 Enzymatic activities

For the glutathionylation tests, three substrates have been tested namely 1-chloro 2,4-dinitrobenzene (CDNB), phenethyl isothiocyanate (PEITC) and benzyl isothiocyanate (BEITC). The measurement of these activities has been done at 25°C by following the absorbance due to the formation of the glutathionylated product: 340 nm in the case of the CDNB and 274 nm for both isothiocyanate compounds. According to the substrate tested, the buffer reaction (in a final volume of 500 µL) was different; a 30 mM Tris-HCl pH 8.0, 1 mM EDTA buffer in the case of the CDNB assays and a 100 mM phosphate buffer pH 6.4 for the isothiocyanate derivatives tests. Several concentrations of CDNB (500 – 3000 µM), PEITC (25 – 500 µM) and BEITC (25 – 500 µM) were used with a fixed concentration of reduced glutathione of 1 mM added in the reaction mixture. To check the reductase and the peroxidase activities of the TvGSTOs, several concentrations of 2-hydroxyethyl

disulfide (HED, 50 – 2000 µM) and cumene hydroperoxide (CuOOH, 100 – 2500 µM) were respectively tested by following the consumption of NADPH (at 340 nm) catalyzed by glutathione reductase. At 25°C, the reaction mixture was composed of a 500 µL of 30 mM Tris-HCl pH 8.0, 1 mM EDTA buffer containing 1 mM of reduced glutathione, 180 µM of NADPH, 0.5 units of yeast glutathione reductase. For all the experiments above, data analysis and the calculations of the kinetic parameters have been performed by using a nonlinear regression model based on the Michaelis-Menten equation with the GraphPad Prism software. Kinetic parameters of TvGSTO1C, 2C and C3 for the deglutathionylation activity towards S-glutathionyl-phenylacetophenone (GS-PAP) have been determined by using high performance liquid chromatography. These enzymatic tests have been done as previously explained (Lallement et al., 2014b).

2.10 Thermal stability assay

These assays were performed as described in Deroy et al. (Deroy et al., 2015) in 96 well microplates (Harshell, Biorad) and the measurements were carried out using a real time PCR detection system (CFX 96 touch, Biorad). The assays were achieved as follows : 5 µL of Tris-HCl (150 mM) pH 8 buffer, 2 µL of molecules (initial concentration of 1250 µM), 5 µL of proteins at a final concentration of 20 µM, 2 µL of SYPRO orange previously diluted 80 fold and 11 µL of ultra-pure water for a total volume of 25 µL per well. The plate was centrifuged 30 seconds at 4000g. The fluorescence was measured (at excitation at 485 nm and emission at 530 nm) each minute starting from 3 minutes at 5°C with temperature increase 1°C per minute up to 95°C. The denaturation temperature (T_d), which corresponds to the temperature where 50% of the highest fluorescence is measured, was determined by using the non-linear regression Boltzmann sigmoidal model with the GraphPad Prism software. For each compound, three replicates have been performed. As a reference, similar experiments were conducted adding only dimethyl sulfoxide (DMSO) corresponding to the T_dRef. The thermal shifts (ΔT_d) of each condition corresponding to the difference between the obtained T_d and the T_dRef were calculated.

2.11 Real-time molecular interaction study

The binding of oxyresveratrol onto TvGSTO2C was investigated in the same condition as previously explained (Perrot et al., 2018), with some modifications. The protein was solubilized at 500 nM in 10 mM sodium phosphate buffer, pH 7.4, containing 40 mM NaCl, 0.05% Tween20, 50 µM EDTA, and 50 µM EGTA (PE40 buffer). Oxyresveratrol at 100 µM in PE40 buffer containing 2% DMSO was injected in a chosen channel of the chip (association kinetics) and then, PE40 buffer containing 2% DMSO was injected (dissociation kinetics). Real-time measurements of kinetics responding to changes to the molecular environment upon analyte binding (oxyresveratrol) gave the association constant (kon) of the interaction. The hydrodynamic diameters (DH) of native and reduced TvGSTOs were determined (n = 4) with the Lollipop mathematical model from molecular dynamics measurements as explained (Langer et al., 2013). All curves were analyzed by nonlinear fitting of single-exponential functions with the switchANALYSIS® software from Dynamic Biosensors.

3 Results and discussion

3.1 Genomic and phylogenetic analysis of GSTOs and GSTXs in the Agaricomycotina

The genomic distributions of the putative genes of Omega (GSTOs) and Xi GSTs (GSTXs, previously included in the Omega class (Morel et al., 2009)) were evaluated from 240 complete genomes of Agaricomycotina species (Supplementary Table S1). 971 GSTO genes and 383 GSTX genes were retrieved (Supplementary Table S1). The comparative genomic analysis revealed that GSTXs were ubiquitous while seventeen genomes contain no GSTO genes as already pointed out in *Saccharomyces cerevisiae* (Schwartz et al., 2016). The number of GSTO genes differs significantly from one species to another (from 0 to 16 genes), with the highest numbers found mainly in Polyporales species such as *Trametes versicolor* (16 genes). This study shows that extension of the number of GSTOs also exists in other orders such as Boletales, Russulales and Hymenochaetales orders (Supplementary Table S1).

Four Polyporales, three Boletales, two Russulales and one Hymenochaetales fungi, showing extension in the number of GSTOs, were selected for a phylogenetic analysis of the Omega and Xi GSTs. The 117 sequences are divided into two main groups that separate GSTXs from GSTOs as expected (Fig. 1). GSTOs can be split into two Types called Type-A and Type-B. The putative catalytic residue of Type-A GSTOs is a cysteine or a serine while the putative catalytic residue of Type-B GSTOs is a cysteine only, as is the case with GSTXs (Fig. 1). This new classification has been applied to the GSTO sequences of the 240 genomes and new notations have been introduced: Type-A contains either serine GSTOs ($GSTOs^{A\text{-}Ser}$) or cysteine GSTOs ($GSTOs^{A\text{-}Cys}$) while Type-B contains only cysteine GSTOs ($GSTOs^{B\text{-}Cys}$) (Supplementary Table S1). In most of cases, when an organism has $GSTO^{A\text{-}Ser}$ genes, it also has cysteine GSTOs (i.e. $GSTOs^{A\text{-}Cys}$ and $GSTOs^{B\text{-}Cys}$). In the genomes with the largest GSTO extensions, the number of $GSTOs^{A\text{-}Ser}$ is always significantly larger than in the other two groups. Indeed, *T. versicolor* genome contains 12 genes of $GSTOs^{A\text{-}Ser}$ (TvGSTO1S to TvGSTO12S), 2 of $GSTOs^{A\text{-}Cys}$ (named TvGSTO1C and TvGSTO2C) and 2 of $GSTOs^{B\text{-}Cys}$ (named TvGSTO3C and TvGSTO4C).

3.2 Transcriptomic study of Trametes versicolor $GSTOs^{A\text{-}Cys}$ and $GSTOs^{B\text{-}Cys}$

With the aim to focus on the expression of genes of $GSTOs^{A\text{-}Cys}$ and $GSTOs^{B\text{-}Cys}$, two *Trametes versicolor* strains have been grown on malt agar medium and their transcriptome analysed (RNAseq) after 14 and 30 growth days. Transcriptomic data that were previously published were added to the analysis of the GST gene expression levels. These supplementary data were obtained with two other *T. versicolor* strains and using different growth media: glucose medium and poplar fibres to identify the enzymes involved in lignocellulose degradation (Zhang et al., 2017) and aspen wafers of different widths in order to simulate a progressive decay gradient (Zhang et al., 2019). As a first step, the whole TvGSTome was analysed. It contains 44 GST-encoding genes, which belong to the classes Omega (12 $GSTO^{A\text{-}Ser}$ genes, 2 $GSTO^{A\text{-}Cys}$ genes and 2 $GSTO^{B\text{-}Cys}$ genes), Ure2p (11 genes), FuA (6 genes), Phi (4 genes), Xi (3 genes), and GTT (1 gene). Two genes encoding eukaryotic translation elongation factor 1Bγ (TvEF1Bγ, Prot ID 72991 and 22196) were added in this study because these constitutive proteins contain a glutathione transferase domain (Le Sourd et al., 2006). For each culture conditions, obtained data (RPKM : Reads Per Kilobase of exon model per Million mapped reads) have been centred-reduced before being subjected to a principal component analysis (Fig. 2A and 2B). The first factor explains more than 67% of the total variance and distributes the GST genes according to their expression in all tested conditions. Indeed, this factor efficiently differentiates 9

highly expressed GSTs, including a TvEF1Bγ gene as expected. A large proportion of GSTs are poorly or not expressed probably because the great majority of TvGSTs are inducible enzymes. The 8 highly expressed GSTs include 5 Type-A TvGSTOs, 2 TvUre2ps and 1 TvGSTF. Interestingly, some Ure2ps are constitutive proteins in the basidiomycete *Phanerochaete chrysosporium* and the phi class is the most expressed GST class in some plant species such as maize (Öztetik, 2008; Roret et al., 2015). The 5 genes that belong to the Omega class comprise those of three TvGSTOs$^{A\text{-}Ser}$ and the 2 TvGSTOs$^{A\text{-}Cys}$ (TvGSTO1C and TvGSTO2C) suggesting their involvement in essential functions during the fungal growth (Supplementary Table S2A). Although both TvGSTOs$^{B\text{-}Cys}$ (TvGSTO3C and TvGSTO4C) belong to the cluster of the weakly expressed GSTs, TvGSTO3C is the furthest away from the cluster center (Fig. 2A). This is explained by the fact that an upregulation of TvGSTO3C was detectable in the wood decay monitoring experiment (Supplementary Table S2A). This first analysis of *T. versicolor* transcriptomes revealed a different behaviour of the genes of GSTOs$^{A\text{-}Cys}$ and GSTOs$^{B\text{-}Cys}$. Larger surveys show that other fungi can share this characteristic. We analysed previously published transcriptomic data from five fungi (*Lentinus tigrus, Coprinopsis cinerrea, Phanerochaete chrysosporium, Schizophyllum pombe, Rickenella mellea*) and focused on the expression of TvGSTOs$^{A\text{-}Cys}$ and TvGSTOs$^{B\text{-}Cys}$ (Krizsan et al., 2019). Data have been centred-reduced before analysis for each fungus and culture conditions (19 genes, three growth conditions). Tukey's test revealed significant differences between the genes of GSTOs$^{A\text{-}Cys}$ and GSTOs$^{B\text{-}Cys}$ ($p<0.0001$) (Fig. 2C). This second transcriptomic analysis is in perfect agreement with the first one. Indeed, each fungus has at least one GSTO$^{A\text{-}Cys}$ isoform that is constitutively expressed, whereas the expression of GSTOs$^{B\text{-}Cys}$ is predominantly lower under the conditions tested (Supplementary Table S2B).

3.3 Crystal structures of two TvGSTOs$^{A\text{-}Cys}$ and one TvGSTO$^{B\text{-}Cys}$

The crystal structures of TvGSTO1C and TvGSTO2C (GSTOs$^{A\text{-}Cys}$ *i.e.* fungal GSTOs from the Type-A that contains a catalytic cysteine) and of TvGSTO3C (GSTOs$^{B\text{-}Cys}$) were determined at near atomic resolution (Supplementary Table S3). We previously solved the crystal structures of three isoforms of GSTOs$^{A\text{-}Ser}$ from *T. versicolor*, which contain a catalytic serine (TvGSTO2S, 3S and 6S) (Perrot et al., 2018; Schwartz et al., 2018). TvGSTOs are V-shaped homodimeric enzymes and their respective monomers adopt the canonical cytosolic GST fold, *i.e.* an N-terminal thioredoxin domain (β1α1β2α2β3β4α3) followed by a bundle of at least 6 α-helices (α4α5α6α7α8α9) (Fig. 3A-C). Whatever the catalytic residue, Type-A TvGSTOs are very similar from a structural point of view (rmsd below 1.0 Å). However, the comparison of Types A and B revealed significant differences (*e.g.* rmsd of 1.68 Å between TvGSTO1C and TvGSTO3C). Only TvGSTO3C contains an extra N-terminal tail, which is folded as a 3-turn helix (α0). It sits on the external side of the monomer along the β-sheet and joins the helix α8 with two hydrogen bonds (Fig. 3C). Analysis of the sequences shows that this helix α0 could be conserved in fungal GSTO3C homologs that belong to Type-B (Supplementary Fig. S1). TvGSTO1C and TvGSTO2C like TvGSTOs$^{A\text{-}Ser}$ (TvGSTO2S, TvGSTO3S and TvGSTO6S) include a proline-rich loop between β3 and β4. In the helix bundle, helix α5 is two turns longer in TvGSTO3C and an additional helix α6' is only present in Type-A GSTOs (Fig. 3B). Additional difference concerns helix α9. In monomer B of TvGSTO3C, it covers the active site and interacts with the covalently bound glutathione (see below). This helix α9 adopts a configuration that keeps the active site open in TvGSTO1C and TvGSTO2C like in TvGSTOs$^{A\text{-}Ser}$. These differences in the C-terminal domain, around the substrate fixation sites (G site and H site), could suggest differences in biochemical properties.

In each structure of the present study, a molecule of glutathione is covalently bound to the catalytic cysteine in each monomer of the homodimers (C13 in TvGSTO1C and 2C, C37 in TvGSTO3C) (Fig. 3D and 3E). The glutathione binding site residues (G-site) are mainly borne by the N-terminal domain and are well conserved between the three isoforms. GSTOs$^{A\text{-}Ser}$ show a similar G-site without the ability to covalently bind the glutathione molecule because these isoforms contain a catalytic serine residue (Schwartz et al., 2018). The C-terminal end of the monomer B of TvGSTO3C helix α9 covers the active site and interacts with the glutathione molecule via the side chains of R238 and Q242 (Fig. 3C and 3E). This helix α9 also forms intermolecular contacts with a symmetry related molecule. No electron density was observed in the equivalent region of monomer A, which is close to a solvent channel of the crystal. This could suggest that TvGSTO3C C-terminal end is folded only in presence of a macromolecular partner.

The H-site of the active site of the GSTs is the binding pocket for the electrophilic substrate or for the adduct moiety of glutathione derivatives. The boundaries of this second pocket are not as easy to define as those of the glutathione site. Several sites are sometimes proposed for one isoform, such as for TvGSTO3S where at least three putative binding sites have been identified for the electrophilic substrate (Schwartz et al., 2018; Schwartz et al., 2019). Two of them mainly involve residues from the C-terminal domain. The first one is a deep, apolar, buried pocket, which is not present in TvGSTO1C, 2C and 3C. The second one, much more solvent accessible, is adjacent to helices α4, α5 and α9 (Fig. 4). A molecule of Hepes in the TvGSTO1C crystal structure occupies the corresponding region (Fig. 4A). The hydroxyl group of the Hepes sulfonic moiety is at 3.0 Å distance from the glutathione sulfur-atom. We solved the crystal structure of TvGSTO2C in complex with the polyphenolic stilbene oxyresveratrol, which occupies roughly the equivalent region between the loop β2-α2 and helix α4 (see below, section “Interaction study of TvGSTO-ligands”) (Fig. 4B). Carbon atoms of the oxyresveratrol double-bond are found at less than 4 Å from the sulfur atom of GSH. This observation questions a putative catalysis with a related substrate. The oxyresveratrol molecule could also reflect the position of the second glutathione molecule required for the TvGSTO2C regeneration. Indeed the crystal structure of an inactive mutant of HsGSTO1 in complex with oxidized glutathione (GSSG) shows that one GS- moiety occupies the expected G site while the second GS-moiety sits in a region quite similar to that of oxyresveratrol molecule in TvGSTO2C (Brock et al., 2013) (Supplementary Fig. S2). Finally, superimposition of the crystal structures of TvGSTO1C, 2C and 3C shows that this large solvent accessible H-site could be shared by the three isoforms (Supplementary Fig. S3).

Regardless of the Type (A or B) of Omega TvGSTs, a search for the structural homologs using Dali (Holm and Laakso, 2016) or PDBeFold (Krissinel and Henrick, 2004) ranked Plant Tau GSTs at the top of the list instead of the expected Animal Omega GSTs. The first six hits were Tau, Delta, Lambda and Omega classes, the stringent starvation protein A (sspA) and a thiol dependent reductase (TDR1), which belongs to the GST superfamily (Fyfe et al., 2012). In an attempt to optimize the structural alignments, we used the new Dali option “all against all structure comparison” because the direct pairwise comparison during the “PDB search” of Dali can result in some gaps and inconsistencies (Holm and Laakso, 2016). The new algorithm generated a structural dendrogram that provided a new point of view on the structural homology of TvGSTOs (Fig. 5). The circular dendrogram separates the selected proteins in two clades. Type-A and B TvGSTOs are in the clade that includes cysteine GSTs (Omega and Lambda classes and TDR1) and Tau GSTs. Crystallographic studies had already mentioned this proximity between the Omega, Lambda and Tau classes and TDR1 (Fyfe et al., 2012;

Lallement et al., 2014b; Thom et al., 2002). Type-A TvGSTOs are closer to animal GSTOs. Our initial analysis based on sequence alignments found the opposite, i.e. a closer proximity between GSTOs$^{B\text{-}Cys}$ and Animal GSTOs, which both contain an N-terminal extension. However, the crystallographic data reveal that these extensions are structurally different, unfolded and in front of the β-sheet in Animal GSTOs while folded in an α-helix that sits along the β-sheet in GSTOs$^{B\text{-}Cys}$ (Board et al., 2000) (Supplementary Fig. S4). The discrepancy between the results of the "PDB search" and the "all against all comparison" can be explained by the high conservation of the scaffold shared by all the members of the cytosolic GST superfamily. All the structures selected from the "PDB search" and used in the "all against all comparison" belong to the "Main" subgroup of GSTs defined by the cytosolic GST classification based on more than 13,000 sequences and therefore are very similar (Mashiyama et al., 2014). This study separates the cytosolic GSTome into at least three subgroups. One of these subgroups consists in mostly eukaryotic GSTs from the well-known Alpha, Mu, Pi, and Sigma classes. The smallest subgroup contains only the Xi class while the largest subgroup, designated as ''Main'', consists in all other defined cytosolic classes.

To summarize, our crystallographic analysis shows that GSTOs$^{A\text{-}Cys}$ and GSTOs$^{B\text{-}Cys}$ have structural features that distinguish them, confirming their separation previously proposed by our phylogenetic analysis (see above) based on sequence information.

3.4 Biochemical characterization

TvGSTO1C, 2C, 3C and 4C were produced as recombinant proteins in *E. coli*. TvGSTO4C was insoluble and was not further characterized. The native forms of TvGSTO1C, 2C and 3C were found glutathionylated as mass spectrometry analysis revealed a covalent adduct of 305 Da. The glutathione was removable after reduction by DTT (Supplementary Table S4). Spectrophotometric measurements based on the cleavage of Ellman's reagent (DTNB) confirmed these observations. TvGSTO1C and TvGSTO2C have one cysteine residue while TvGSTO3C contains two. No free thiol group was detected in the native forms of TvGSTO1C and TvGSTO2C, and only one in TvGSTO3C. All the cysteine thiol groups were accessible after a reduction treatment (Supplementary Table S4).

The enzymatic activities of TvGSTO1C, 2C and 3C were assessed with three electrophilic substrates (CDNB, PEITC and BEITC), a peroxide compound (CuOOH), a disulfide substrate (HED) and a glutathione derivative (GS-PAP) (Table 1, Supplementary Fig. S5). We have also determined the kinetic parameters of six TvGSTOs$^{A\text{-}Ser}$ (TvGSTO1S, 2S, 3S, 4S, 5S, and 6S, which contain a catalytic serine residue). The latter have the ability to transfer the glutathione molecule to the electrophilic-substrates whereas TvGSTO1C, 2C and 3C cannot, as expected. These three enzymes do not have peroxidase activity towards CuOOH. In general, they exhibit quite similar catalytic properties to those of cysteine GSTOs from *P. chrysosporium* (PcGSTO3C and PcGSTO4C) and *H. sapiens* (HsGSTO1) (Board and Menon, 2016; Meux et al., 2013; Meux et al., 2011). TvGSTO1C, 2C and 3C show reductase activities against GS-PAP and HED. Whatever the Type (A or B), the catalytic efficiency ($kcat/K_M$) is higher for the deglutathionylation activity than the thioltransferase activity. TvGSTO3C shows the best catalytic efficiencies for the two substrates because it almost has the best catalytic turnover rates (Table 1).

3.5 Interaction study of TvGSTOs-Ligands

Recently, thermal shift assays (TSA) have allowed us to establish that polyphenolic compounds are ligands of TvGSTOs$^{A\text{-}Ser}$ (Cimmperman and Matulis, 2011; Perrot et al., 2018;

Schwartz et al., 2018). These ligands bind either in the active site or in the ligandin binding site located at the interface of the homodimer (L-site). We show in this section that TvGSTO1C, 2C and 3C retain this ability. Ten flavonoids (including two glycosylated ones) and one stilbene were screened against the native and reduced forms of TvGSTO1C, 2C and 3C. First, the denaturation temperature is highly dependent on the redox state of the isoform. Indeed, the denaturation temperature (Td) of the native form is at least 18°C higher than in the reduced form (Supplementary Table S5). These results clearly show that the presence of a covalently bound glutathione greatly stabilizes TvGSTO1C, 2C and 3C, as might have been expected.

TSA show that each isoform has its own polyphenol interaction profile as observed for TvGSTOs$^{A\text{-}Ser}$ (Schwartz et al., 2018). The interaction profiles of TvGSTO1C and 2C are redox state-dependent (Fig. 6 and Supplementary Fig. S6). Most of the polyphenolic compounds stabilize the native forms while they destabilize the reduced ones. The main difference between TvGSTO1C and 2C lies in the magnitude of the thermal shifts (ΔTd), with the largest positive values observed for the native form of TvGSTO1C. In the case of TvGSTO3C, the ΔTds do not appear to be dependent on the redox state of the protein, although the magnitudes do not exceed 2°C. Among all compounds, the greatest amplitude of the shift is observed for the TvGSTO1C denaturation temperature with the flavonoid quercetin (ΔTd = + 4.0 °C). We failed to obtain a crystal structure of TvGSTO1C in complex with quercetin even though such a structure was recently published for a plant GST Phi (Ahmad et al., 2017). In this study, the crystal structure revealed two new ligandin sites, which did not appear well conserved among plant GSTs. Naringenin is also an interesting compound because it stabilizes, to a lesser extent, the three isoforms TvGSTO1C, 2C and 3C. We were able to obtain a crystal structure of TvGSTO2C in complex with naringenin as we succeeded earlier with a TvGSTO$^{A\text{-}Ser}$ (TvGSTO6S) (Schwartz et al., 2018). Like in the latter, a pair of naringenin molecules was found in the L-site at the dimer interface (Fig. 3A). A structural analysis revealed that TvGSTO1C and 3C most likely contained this L site (Supplementary Fig. S7). However, entering this site requires conformational changes of a few side chains. Interestingly, Brock and coll. (Brock et al., 2013) found a glutathione derivative in this L-site in the human GSTO1 (HsGSTO1) and proposed that it could represent the binding location for uncompetitive inhibitors. All these data suggest that GSTOs contain a conserved ligandin binding site deep within the dimer interface of these enzymes.

Our previous studies and the present one clearly show that a small positive ΔTd can be significant (Schwartz et al., 2018). The stilbene oxyresveratrol induced a weak but specific stabilizing effect on the native form of TvGSTO2C (ΔTd = + 0.7°C) when destabilization was observed in the reduced form (ΔTd = - 0.8°C). The interaction has been investigated more accurately using the switchSENSE technology (Supplementary Fig. S8). In accordance with the TSA, the association rate constants for oxyresveratrol binding depend on the redox state of TvGSTO2C. If the k_{on} of the native form (361 ± 73 $M^{-1}.s^{-1}$) is the highest, the reduced form also interacts with oxyresveratrol (k_{on} 88 ± 26 $M^{-1}.s^{-1}$). Unfortunately, the oxyresveratrol dissociation was not observable for both redox states. The stilbene was successfully soaked with the crystals of the TvGSTO2C native form. The oxyresveratrol molecule occupies the H-site described above in an extended *trans* configuration with most of its hydroxyl groups hydrogen bonded to TvGSTO2C side chains and the glutathione molecule. The involvement of glutathione in the binding of oxyresveratrol could explain the better affinity of the native form for the ligand. In a previous study, the TSA allowed us to detect oxyresveratrol in an Amazonian wood species, using a TvGSTO$^{A\text{-}Ser}$ (TvGSTO2S) as the probe (Perrot et al., 2018). From this observation, we had solved the crystal structure of TvGSTO2S in complex with pure oxyresveratrol

and measured a k_{on} of 141 ± 18 $M^{-1}.s^{-1}$. Therefore, these results suggest that TvGSTOs$^{A\text{-}Cys}$ possess properties for binding wood polyphenolic compounds similar to TvGSTOs$^{A\text{-}Ser}$.

4 Conclusions

This article first presented an update on the nomenclature of the GST Omega class in mushroom-forming fungi (GSTOs). Fungal GSTOs can be divided phylogenetically into Type-A and B. The catalytic residue of Type-A GSTOs is either cysteine (GSTOs$^{A\text{-}Cys}$) or serine (GSTOs$^{A\text{-}Ser}$) and that of Type-B GSTOs is only cysteine (GSTOs$^{B\text{-}Cys}$). GSTO genes are found in almost all the analyzed Agaricomycotina genomes. As previously shown, they are mainly widespread in Polyporales order, but also in Boletales, or Russulales orders. When a genome contains a large number of GSTOs, GSTOs$^{A\text{-}Ser}$ are always the most abundant. It has been suggested that GSTOs$^{A\text{-}Ser}$ could have a role in the polyphenols transport because most have a ligandin binding site (L-site) at the dimer interface (Perrot et al., 2018; Schwartz et al., 2018). Interestingly, GSTOs$^{A\text{-}Cys}$ and GSTOs$^{B\text{-}Cys}$ have this L site, which appears as a conserved structural feature of fungal GSTOs.

Although Type-A and B GSTOs adopt the GST canonical fold, they exhibit significant structural differences and Type-A would be the closest to mammalian GSTOs. Our analysis of the transcriptomes of six diverse fungal organisms under a variety of conditions points to a difference between the two Types of cysteine GSTOs. GSTOs$^{A\text{-}Cys}$ would be constitutive enzymes, while GSTOs$^{B\text{-}Cys}$ would be inducible ones. The metabolic role(s) of GSTOs$^{A\text{-}Cys}$ remain(s) to be elucidated. Several are now established for their human counterparts such as in the ubiquitous glutathionylation cycle, in which GSTOs$^{A\text{-}Cys}$ could play a role (Menon and Board, 2013).

If structural studies and transcriptomic analyses clearly distinguished Type-A and -B GSTOs, biochemical results did not. Indeed, all fungal cysteine GSTOs in this and other studies have the same catalytic profile, which is similar to that of the human isoform HsGSTO1. These enzymes reduce glutathione derivatives such as GS-PAP as well as the disulfide bridge of HED. Organisms like *Trametes versicolor* arm themselves with multiple isoforms of detoxification enzymes to cope with unpredictable environmental variations. But why have multiple isoforms of cysteine GSTOs to perform the same task? These enzymes could have specific substrates yet to be discovered because the tests have been carried out with laboratory substrates, as already mentioned (Mashiyama et al., 2014). Tomanek and coll. (Tomanek et al., 2020) have very recently proposed another answer. Their study suggests that bacteria, when facing new environments, more readily use the products of gene duplications rather than adapting their transcriptional machinery. Indeed, efficient regulation processes may take a long time to set up (Tugrul et al., 2015). Hitherto underestimated, this attractive model is proposed to be valid in all kingdoms of life (Tomanek et al., 2020) and could apply to our case.

Databases

Structural data is available in Protein Data Bank (PDB) database under the accession code numbers **6HJS**, **6SR8**, **6SR9**, **6SRA** and **6SRB**.

Conflicts of interest

The authors declare no conflict of interest.

Acknowledgments

The authors would like to thank ESRF for beamtime, and the staffs of beamlines FIP-BM30A and ID30B for assistance with crystal testing and data collection. The authors appreciated the access to the 'Plateforme de mesures de diffraction X' of the Université de Lorraine. The authors declare no competing financial interest. Real-time biomolecular interactions were investigated with the switchSENSE® technology available on the ASIA platform (Université de Lorraine-INRAE, https://a2f.univ-lorraine.fr/asia/). This study was funded by the French National Research Agency (ANR-11-LABX-0002-01), the Centre National de la Recherche Scientifique, the University of Lorraine and the Région Grand Est (MS and TP Grants, PEPS-Mirabelle 2016, CPER 2014-2020).

References

Ahmad, L., et al., 2017. Structural evidence for Arabidopsis glutathione transferase AtGSTF2 functioning as a transporter of small organic ligands. FEBS Open Bio. 7**,** 122-132.

Board, P. G., 2011. The omega-class glutathione transferases: structure, function, and genetics. Drug Metab Rev. 43**,** 226-35.

Board, P. G., et al., 2000. Identification, characterization, and crystal structure of the omega class glutathione transferases. Journal of Biological Chemistry. 275**,** 24798-24806.

Board, P. G., Menon, D., 2016. Structure, function and disease relevance of Omega-class glutathione transferases. Arch Toxicol. 90**,** 1049-67.

Brock, J., et al., 2013. Structural Insights into Omega-Class Glutathione Transferases: A Snapshot of Enzyme Reduction and Identification of a Non-Catalytic Ligandin Site. PLoS ONE. 8**,** 1-10.

Campanella, J. J., et al., 2003. MatGAT: An application that generates similarity/identity matrices using protein or DNA sequences. BMC Bioinformatics. 4**,** 29.

Cimmperman, P., Matulis, D., Chapter 8 Protein Thermal Denaturation Measurements via a Fluorescent Dye. Biophysical Approaches Determining Ligand Binding to Biomolecular Targets: Detection, Measurement and Modelling. The Royal Society of Chemistry, 2011, pp. 247-274.

Davis, I. W., et al., 2004. MOLPROBITY: structure validation and all-atom contact analysis for nucleic acids and their complexes. Nucleic Acids Res. 32**,** W615-9.

Deponte, M., 2013. Glutathione catalysis and the reaction mechanisms of glutathione-dependent enzymes. Biochim Biophys Acta. 1830**,** 3217-66.

Deroy, A., et al., 2015. The GSTome Reflects the Chemical Environment of White-Rot Fungi. PLoS One. 10**,** e0137083.

Emsley, P., Cowtan, K., 2004. Coot: model-building tools for molecular graphics. Acta Crystallogr D Biol Crystallogr. 60**,** 2126-32.

Evans, P. R., Murshudov, G. N., 2013. How good are my data and what is the resolution? Acta Crystallogr D Biol Crystallogr. 69**,** 1204-14.

Fyfe, P. K., et al., 2012. Leishmania TDR1 structure, a unique trimeric glutathione transferase capable of deglutathionylation and antimonial prodrug activation. Proceedings of the National Academy of Sciences. 109**,** 11693.

Hayes, J. D., et al., Glutathione transferases. Vol. 45, 2005, pp. 51-88.

Holm, L., Laakso, L. M., 2016. Dali server update. Nucleic Acids Res. 44**,** W351-5.

Hughes, M. M., et al., 2019. Glutathione Transferase Omega-1 Regulates NLRP3 Inflammasome Activation through NEK7 Deglutathionylation. Cell Rep. 29**,** 151-161 e5.

Kabsch, W., 2010. XDS. Acta Crystallographica Section D: Biological Crystallography. 66**,** 125-132.

Krissinel, E., Henrick, K., 2004. Secondary-structure matching (SSM), a new tool for fast protein structure alignment in three dimensions. Acta Crystallogr D Biol Crystallogr. 60**,** 2256-68.

Krizsan, K., et al., 2019. Transcriptomic atlas of mushroom development reveals conserved genes behind complex multicellularity in fungi. Proc Natl Acad Sci U S A. 116**,** 7409-7418.

Lallement, P.-A., et al., 2014a. The still mysterious roles of cysteine-containing glutathione transferases in plants. Frontiers in Pharmacology. 5.

Lallement, P. A., et al., 2014b. Structural and enzymatic insights into Lambda glutathione transferases from Populus trichocarpa, monomeric enzymes constituting an early divergent class specific to terrestrial plants. Biochemical Journal. 462**,** 39-52.

Langer, A., et al., 2013. Protein analysis by time-resolved measurements with an electro-switchable DNA chip. Nat Commun. 4**,** 2099.

Le Sourd, F., et al., 2006. eEF1B: At the dawn of the 21st century. Biochim Biophys Acta. 1759**,** 13-31.

Letunic, I., Bork, P., 2019. Interactive Tree Of Life (iTOL) v4: recent updates and new developments. Nucleic Acids Res. 47**,** W256-W259.

Liebschner, D., et al., 2019. Macromolecular structure determination using X-rays, neutrons and electrons: recent developments in Phenix. Acta Crystallogr D Struct Biol. 75**,** 861-877.

Mashiyama, S. T., et al., 2014. Large-scale determination of sequence, structure, and function relationships in cytosolic glutathione transferases across the biosphere. PLoS Biol. 12**,** e1001843.

Mathieu, Y., et al., 2012. Characterization of a Phanerochaete chrysosporium Glutathione Transferase Reveals a Novel Structural and Functional Class with Ligandin Properties. Journal of Biological Chemistry. 287**,** 39001-39011.

Mathieu, Y., et al., 2013. Diversification of Fungal Specific Class A Glutathione Transferases in Saprotrophic Fungi. Plos One. 8.

McTigue, M. A., et al., 1995. Crystal Structures of a Schistosomal Drug and Vaccine Target: Glutathione S-Transferase fromSchistosoma japonicaand its Complex with the Leading Antischistomal Drug Praziquantel. Journal of Molecular Biology. 246**,** 21-27.

Menon, D., Board, P. G., 2013. A role for glutathione transferase Omega 1 (GSTO1-1) in the glutathionylation cycle. J Biol Chem. 288**,** 25769-79.

Meux, E., et al., 2013. New substrates and activity of Phanerochaete chrysosporium Omega glutathione transferases. Biochimie. 95**,** 336-46.

Meux, E., et al., 2011. Glutathione Transferases of Phanerochaete chrysosporium : S-GLUTATHIONYL-p-HYDROQUINONE REDUCTASE BELONGS TO A NEW STRUCTURAL CLASS Journal of Biological Chemistry. 286**,** 9162-9173.

Morel, M., et al., 2013. Xenomic networks variability and adaptation traits in wood decaying fungi. Microb Biotechnol. 6**,** 248-63.

Morel, M., et al., 2009. The fungal glutathione S-transferase system. Evidence of new classes in the wood-degrading basidiomycete Phanerochaete chrysosporium. Cellular and Molecular Life Sciences. 66**,** 3711-3725.

Nagy, L. G., et al., 2016. Genetic Bases of Fungal White Rot Wood Decay Predicted by Phylogenomic Analysis of Correlated Gene-Phenotype Evolution. Molecular Biology and Evolution. 34**,** 35-44.

Osman, W. H. W., et al., 2018. Characterization of the glutathione S-transferases that belong to the GSTFuA class in Ceriporiopsis subvermispora: Implications in intracellular detoxification and metabolism of wood-derived compounds. International Journal of Biological Macromolecules. 113**,** 1158-1166.

Öztetik, E., 2008. A tale of plant Glutathione S-transferases: Since 1970. Botanical Review. 74**,** 419-437.

Perrot, T., et al., 2018. Fungal Glutathione Transferases as Tools to Explore the Chemical Diversity of Amazonian Wood Extractives. ACS Sustainable Chemistry & Engineering.

Roret, T., et al., 2015. Evolutionary divergence of Ure2pA glutathione transferases in wood degrading fungi. Fungal Genet Biol.

Rozewicki, J., et al., 2019. MAFFT-DASH: integrated protein sequence and structural alignment. Nucleic Acids Res. 47**,** W5-W10.

Schwartz, M., et al., 2016. Crystal Structure of Saccharomyces cerevisiae ECM4, a Xi-Class Glutathione Transferase that Reacts with Glutathionyl-(hydro)quinones. Plos One. 11**,** e0164678.

Schwartz, M., et al., 2018. Molecular recognition of wood polyphenols by phase II detoxification enzymes of the white rot Trametes versicolor. Scientific Reports. 8.

Schwartz, M., et al., 2019. The structure of Trametes versicolor glutathione transferase Omega 3S bound to its conjugation product glutathionyl-phenethylthiocarbamate reveals plasticity of its active site. Protein Science. 28**,** 1143-1150.

Syed, K., et al., 2014. Systematic Identification and Evolutionary Analysis of Catalytically Versatile Cytochrome P450 Monooxygenase Families Enriched in Model Basidiomycete Fungi. PLOS ONE. 9**,** e86683.

Tamura, K., et al., 2013. MEGA6: Molecular Evolutionary Genetics Analysis version 6.0. Mol Biol Evol. 30**,** 2725-9.

Thom, R., et al., 2002. Structure of a tau class glutathione S-transferase from wheat active in herbicide detoxification. Biochemistry. 41**,** 7008-7020.

Thuillier, A., et al., 2014. Transcriptomic Responses of Phanerochaete chrysosporium to Oak Acetonic Extracts: Focus on a New Glutathione Transferase. Applied and Environmental Microbiology. 80**,** 6316-6327.

Thuillier, A., et al., 2013. Atypical features of a Ure2p glutathione transferase from Phanerochaete chrysosporium. FEBS Lett. 587**,** 2125-30.

Tomanek, I., et al., 2020. Gene amplification as a form of population-level gene expression regulation. Nat Ecol Evol. 4**,** 612-625.

Tugrul, M., et al., 2015. Dynamics of Transcription Factor Binding Site Evolution. PLoS Genet. 11**,** e1005639.

Vagin, A., Teplyakov, A., 2010. Molecular replacement with MOLREP. Acta Crystallographica Section D. 66**,** 22-25.

Vince, R., et al., 1971. Inhibition of glyoxalase I by S-substituted glutathiones. Journal of Medicinal Chemistry. 14**,** 402-404.

Whitbread, A. K., et al., Characterization of the omega class of glutathione transferases. Methods in Enzymology, Vol. 401, 2005, pp. 78-99.

Winn, M. D., et al., 2011. Overview of the CCP4 suite and current developments. Acta Crystallogr D Biol Crystallogr. 67**,** 235-42.

Xie, Y., et al., 2020. Development of Benzenesulfonamide Derivatives as Potent Glutathione Transferase Omega-1 Inhibitors. Journal of Medicinal Chemistry.

Zhang, J., et al., 2019. Gene Regulation Shifts Shed Light on Fungal Adaption in Plant Biomass Decomposers. mBio. 10.

Zhang, L., et al., 2017. Transcriptomic Profile of Lignocellulose Degradation from Trametes versicolor on Poplar Wood. BioResources; Vol 12, No 2 (2017).

Table 1

	CDNB	PEITC	BEITC	CuOOH	HED	GS-PAP
K_M (µM)						
TvGSTO1S	(2.03 ± 0.21) E+03	80.8 ± 6.8	48.0 ± 3.4	630 ± 52	ND	ND
TvGSTO2S	765 ± 76	29.7 ± 2.8 (γ)	15.3 ± 1.7	(1.33 ± 0.12) E+03	ND	ND
TvGSTO3S	898 ± 85 (*)	12.2 ± 1.4 (*)	10.3 ± 1.1 (¤)	ND	ND	ND (*)
TvGSTO4S	(2.90 ± 0.38) E+03	21.5 ± 3.1	26.2 ± 2.4	(1.11 ± 0.16) E+04	ND	ND
TvGSTO5S	(3.09 ± 0.22) E+03	77.6 ± 8.1	148 ± 10	(2.10 ± 0.15) E+03	ND	ND
TvGSTO6S	910 ± 87 (*)	24 ± 3 (*)	13.3 ± 2.4	244 ± 28	664 ± 55	ND (*)
TvGSTO1C	ND	ND	ND	ND	(1.33 ± 0.28) E+03	305 ± 52
TvGSTO2C	ND	ND	ND	ND	105 ± 16	817.9 ± (1.8) E+02
TvGSTO3C	ND	ND	ND	ND	200 ± 25	365.8 ± (1.7) E+02
k_{cat} (s^{-1})						
TvGSTO1S	6.04 ± 0.27	6.45 ± 0.19	11.35 ± 0.22	1.56 ± 0.05	ND	ND
TvGSTO2S	0.21 ± 0.01	12.04 ± 0.26 (γ)	32.65 ± 0.62	1.19 ± 0.05	ND	ND
TvGSTO3S	26.67 ± 0.95 (*)	3.08 ± 0.05 (*)	2.80 ± 0.06 (¤)	ND	ND	ND (*)
TvGSTO4S	0.42 ± 0.03	0.39 ± 0.01	3.06 ± 0.07	1.25 ± 0.11	ND	ND
TvGSTO5S	1.26 ± 0.04	0.75 ± 0.02	1.34 ± 0.04	0.70 ± 0.02	ND	ND
TvGSTO6S	4.94 ± 0.17 (*)	11.39 ± 0.36 (*)	11.58 ± 0.64	1.60 ± 0.05	0.12 ± (4.4 E-03)	ND (*)
TvGSTO1C	ND	ND	ND	ND	0.51 ± 0.06	7.0 ± 0.4
TvGSTO2C	ND	ND	ND	ND	0.46 ± 0.02	30.5 ± 3.3
TvGSTO3C	ND	ND	ND	ND	2.41 ± 0.08	15.33 ± 0.52
k_{cat} /K_M ($M^{-1}.s^{-1}$)						
TvGSTO1S	(2.97 ± 0.13) E+03	(7.98 ± 0.23) E+04	(2.37 ± 0.05) E+05	(2.47 ± 0.07) E+03	ND	ND
TvGSTO2S	276.3 ± 9.3	(4.05 ± 0.09) E+05 (γ)	(2.13 ± 0.04) E+06	887 ± 39	ND	ND
TvGSTO3S	(2.97 ± 0.11) E+04 (*)	(2.53 ± 0.42) E+05(*)	(2.72 ± 0.06) E+05 (¤)	ND	ND	ND (*)
TvGSTO4S	146 ± 11	(1.80 ± 0.04) E+04	(1.17 ± 0.03) E+05	111 ± 10	ND	ND
TvGSTO5S	408 ± 14	(9.67 ± 0.22) E+03	(9.02 ± 0.24) E+03	331 ± 10	ND	ND
TvGSTO6S	(5.43 ± 0.18) E+03 (*)	(4.65 ± 0.15) E+05 (*)	(8.69 ± 0.49) E+05	(6.59 ± 0.20) E+03	180 ± 6	ND (*)
TvGSTO1C	ND	ND	ND	ND	382 ± 44	(2.29 ± 0.13) E+04
TvGSTO2C	ND	ND	ND	ND	(4.42 ± 0.17) E+03	(3.74 ± 0.07) E+04
TvGSTO3C	ND	ND	ND	ND	(1.21 ± 0.04) E+04	(4.19 ± 0.13) E+04

Kinetic parameters of the nine studied TvGSTO towards six substrates. All values have been obtained from the GraphPad Prism software by using the non-linear regression representation based on the Michaelis-Menten model. The tested substrates are summarized as follow: “CDNB” for 1-chloro-2,4-dinitrobenzene, “PEITC” for phenethyl isothiocyanate, “BEITC” for benzyl isothiocyanate, “CuOOH” for cumene hydroperoxide, “HED” for 2-hydroxyethyl disulfide and “GS-PAP” for glutathionyl-phenylacetophenone. ND means no activity has been detected. The values accompanied of (*), (γ), (¤) have been obtained in previous works: [18], [19] and [31] respectively. The other values have been determined in this study.

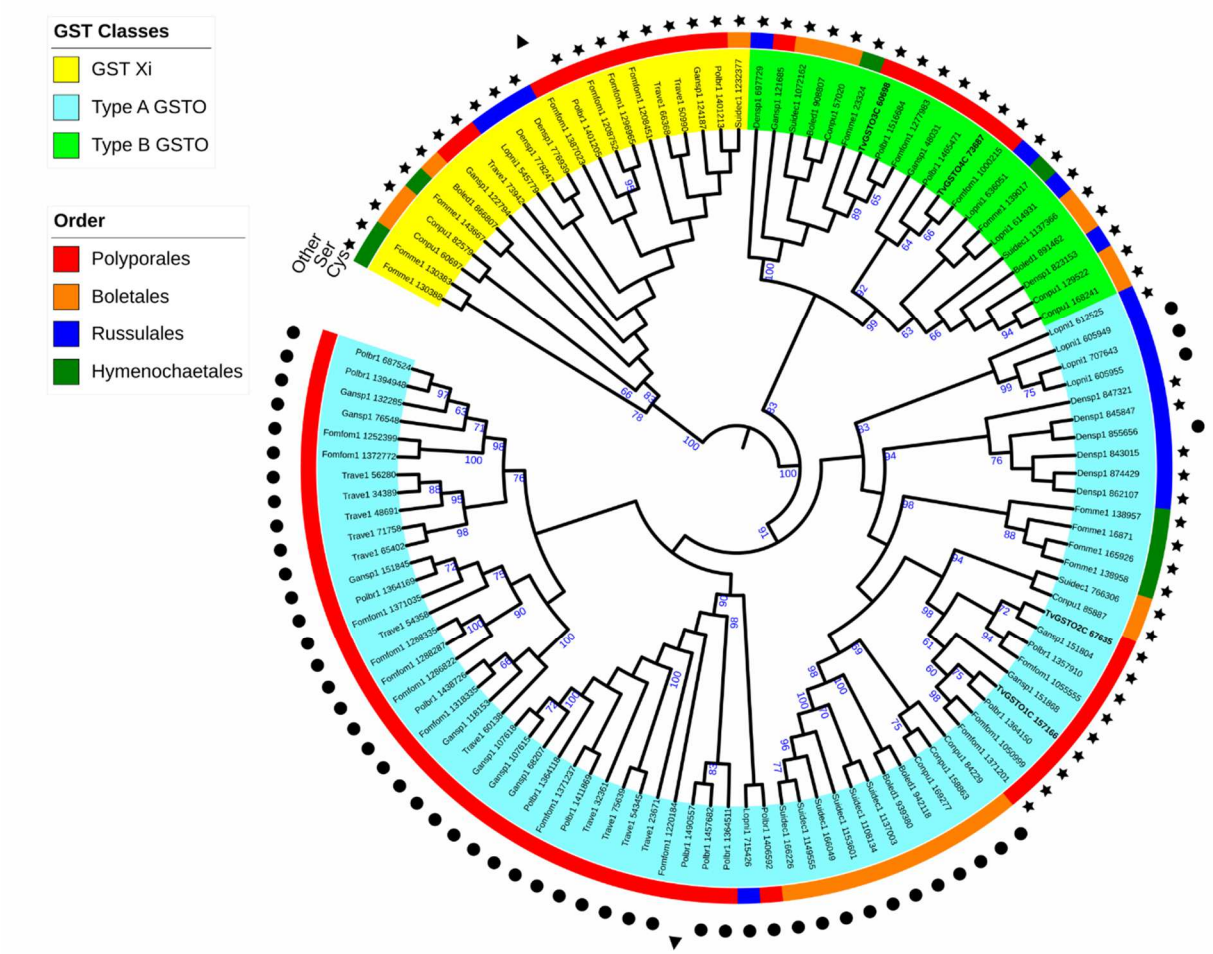

Fig. 1. Circular phylogenetic tree of Xi and Omega GSTs in the Agaricomycotina. Protein sequences were aligned using MAFFT program and a phylogenetic tree was constructed using the neighbor-joining method with the bootstrap resampling number set at 1000. Bootstrap values over 60% are shown above the nodes. The JGI ID number of each selected protein is provided. GSTXs, Type-A and Type-B GSTOs are marked by a different color. Trametes versicolor GSTOs are written in bold characters. The colors of the outer ring corresponds to the Agaricomycotina orders. The putative catalytic residue of each GST is indicated by a symbol : star, cysteine residue; dot, serine residue; triangle, other residues.

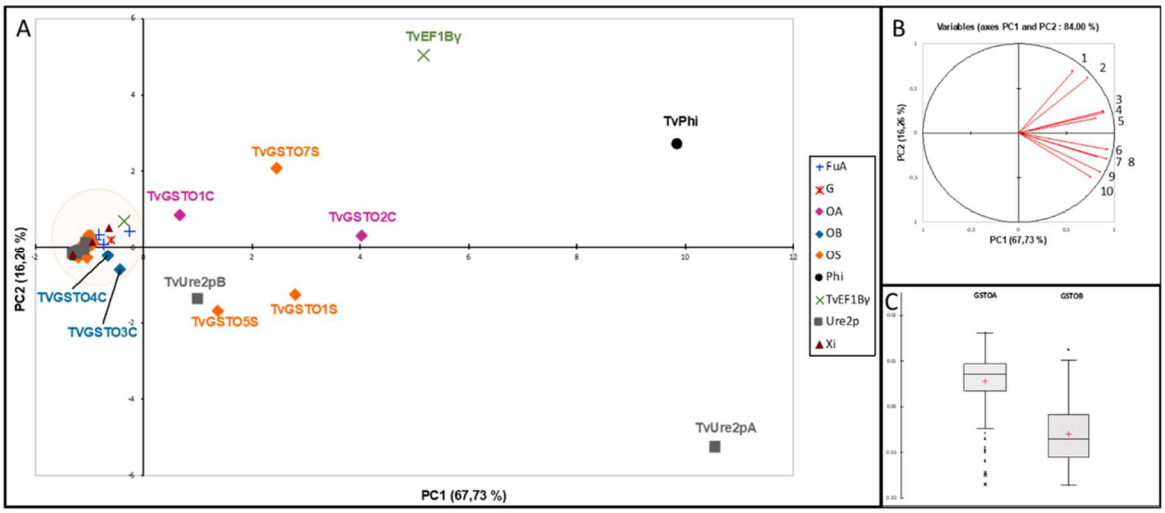

Fig. 2. Expression analysis of GSTome. A principal component analysis has been performed using transcriptomic data obtained from 10 culture conditions using four different *Trametes versicolor* strains. The distribution of the TvGSTs from PC1 and PC2 is shown in A, whereas the variables contribution (see Supplementary Table S2A for more details) is given in B. Analysis of the expression data (C) of GSTOs$^{A\text{-}Cys}$ and GSTOs$^{B\text{-}Cys}$ encoding genes from five fungi (see Supplementary Table S2B for more details) revealed a significant lower expression of the latter (Tukey test ; $p<0.0001$)

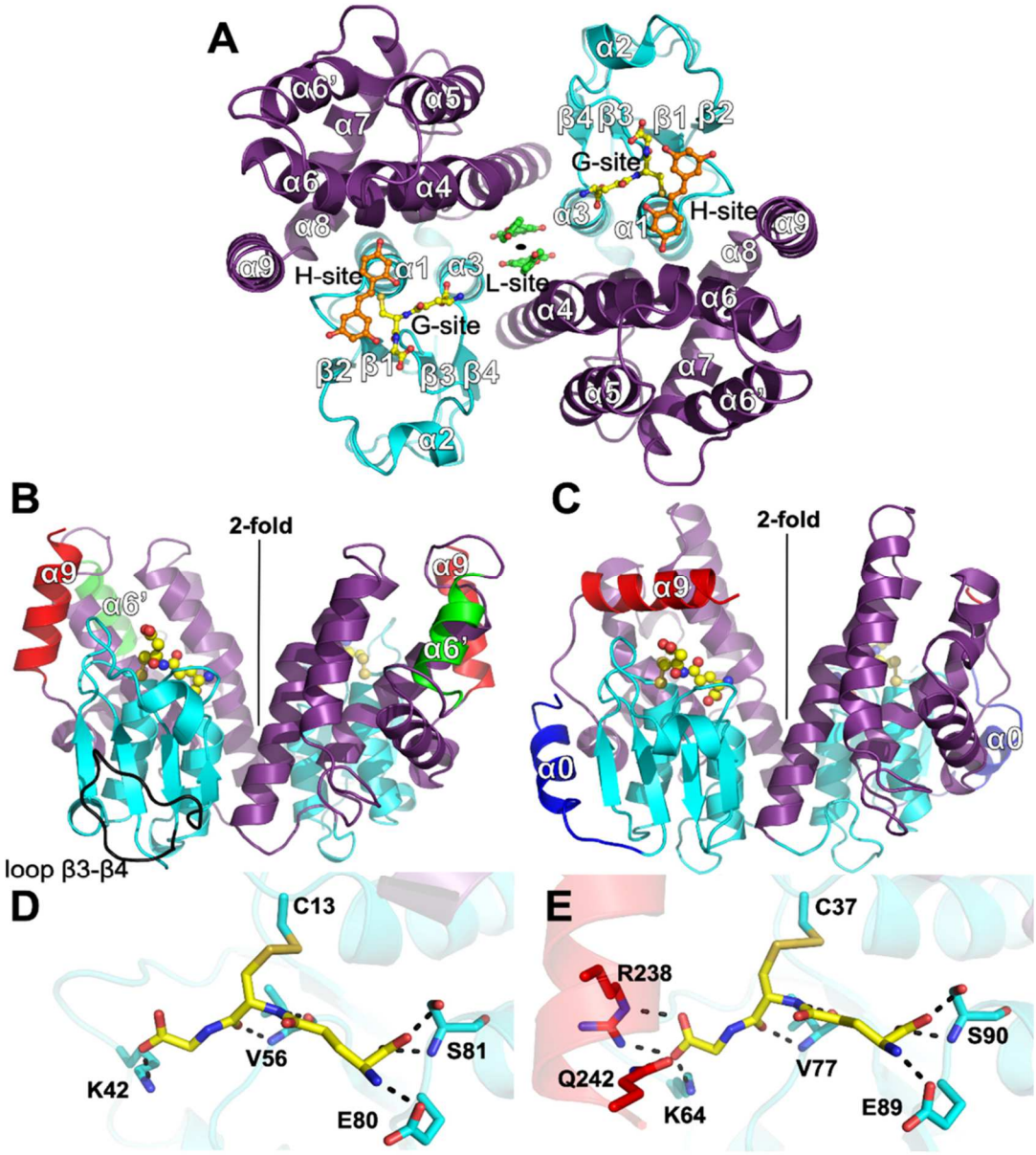

Fig. 3. *Trametes versicolor* Cys-GSTO crystal structures and differences between Type-A GSTOs and Type-B GSTOs **A.** Overall top view of TvGSTO2C dimer. Thioredoxin domain is colored cyan and all-helical domain is colored violet. Glutathione present in the structure is colored yellow. Ligands oxyresveratrol (orange) and naringenin (green) are represented after structural superimposition of TvGSTO2C with solved ligand-bound structures. Corresponding binding sites are labeled. 2-fold axis is shown as a black circle. **B.** Profile view of Type-A TvGSTO2C. Extension between β3-β4 is colored black. Additional helix α6' is colored green. Helix α9 is colored red. GSH is represented as yellow sticks and spheres. **C.** Profile view of Type-B TvGSTO3C. Additional helix α0 is colored blue. Helix α9 is colored red. **D. and E.** Glutathione binding site residues of TvGSTO2C and TvGSTO3C, respectively. Hydrogen bonds are represented as dashed lines.

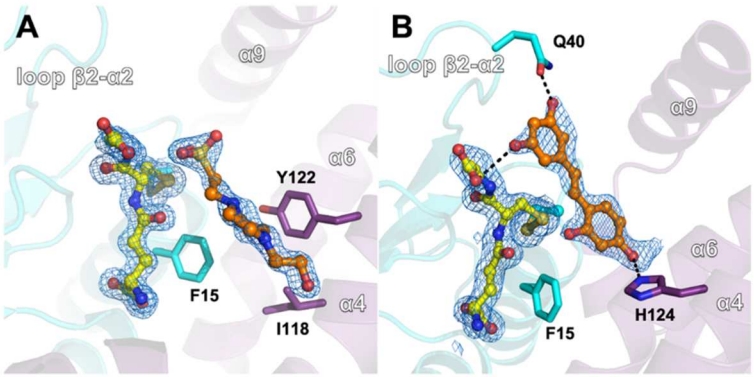

Fig. 4. A. TvGSTO1C bound to a HEPES crystallization buffer molecule (colored orange). **B.** TvGSTO2C bound to an oxyresveratrol molecule (colored orange). GSH is colored yellow. 2mFo-DFc electron density maps are contoured at 1.2 σ. Surrounding residues are represented as sticks and labelled. Ligands are represented as sticks and spheres. Protein structure is represented as cartoon. Hydrogen bonds are represented as dashed lines.

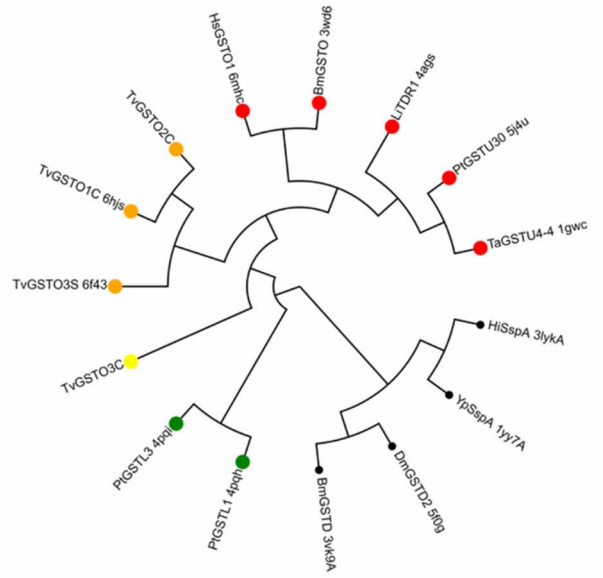

Fig. 5. Circular dendrogram of TvGSTOs and structural homologs. The dendrogram is derived by average linkage clustering of the structural similarity matrix by the DALI server. The dendrogram separates the selected proteins in two clades (big and small leaf dots). Available PDB IDs are provided. TvGSTO1C, TvGSTO2C, TvGSTO3S and TvGSTO3C Glutathione transferase Omega 1C, 2C, 3S and 3C from *Trametes versicolor* ; TaGSTU4-4 glutathione transferase Tau 4-4 from *Aegilops tauschii* ; PtGSTU30 glutathione S-transferase Tau30 from *Populus trichocarpa* ; LiTDR1 Thiol-dependent reductase I from *Leishmania infantum* ; BmGSTO glutathione transferase Omega from *Bombyx mori* ; HsGSTO1 glutathione transferase Omega1 from *Homo sapiens* ; PTGSTL1 and PtGSTL3 glutathione transferase lambda1 and lambda2 from *Populus trichocarpa* ; BmGSTD3 glutathione transferase delta from *Bombyx mori* ; *DmGSTD2* glutathione transferase delta 2 from *Drosophila melanogaster* ; YpSspA stringent starvation protein A from *Yersinia pestis* ; HiSspA stringent starvation protein A homolog from *Haemophilus influenza*.

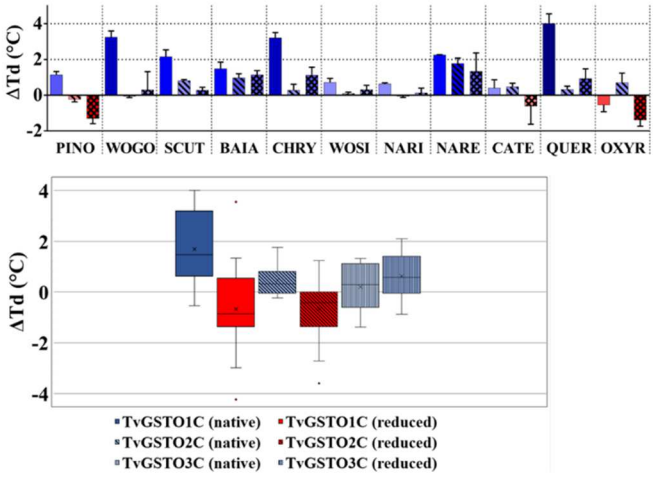

Fig. 6. A. Effects of ten flavonoids and one stilbene on the denaturation temperature (Td) of the native form of three TvGSTOC : full bars for TvGSTO1C, bars with diagonals for TvGSTO2C and bars with crossed lines for TvGSTO3C. **B.** Representation of overall thermal shift (ΔTd) for the three TvGSTOC according to their redox states (native and reduced). The median and the mean are respectively represented by a horizontal line and a cross. For both figures, the positive thermal shifts meaning to stabilizing effects, are represented in blue in contrary to the destabilizing effects (negative ΔTd) represented in red. Higher is the absolute value of the thermal shift, darker is the colour.